HHS Public Access

Author manuscript

Curr Biol. Author manuscript; available in PMC 2020 September 09.

Published in final edited form as:

Curr Biol. 2019 September 09; 29(17): 2826–2839.e4. doi:10.1016/j.cub.2019.07.021.

Mechanical stabilization of the glandular acinus by linker of nucleoskeleton and cytoskeleton complex

Qiao Zhang[1,#], **Vani Narayanan**[2,#], **Keeley L. Mui**[3], **Christopher S. O'Bryan**[4], **Ruthellen H. Anderson**[5], **Birendra KC**[5], **Jolene I. Davis**[2], **Kevin B. Denis**[2], **Susumu Antoku**[3], **Kyle J. Roux**[5,6], **Richard B. Dickinson**[1], **Thomas E. Angelini**[4], **Gregg G. Gundersen**[3], **Daniel E. Conway**[2,*], **Tanmay P. Lele**[1,*,†]

[1.]Department of Chemical Engineering, University of Florida, Gainesville, FL 32611, USA

[2.]Department of Biomedical Engineering, Virginia Commonwealth University, Richmond, VA 23284, USA

[3.]Department of Pathology and Cell Biology, Vagelos College of Physicians and Surgeons, Columbia University, New York, NY 10032, USA

[4.]Department of Mechanical and Aerospace Engineering, University of Florida, FL 32611

[5.]Enabling Technologies Group, Sanford Research, Sioux Falls, SD 57104, USA

[6.]Department of Pediatrics, Sanford School of Medicine, University of South Dakota, Sioux Falls, SD 57105, USA

Summary

The nucleoskeleton and cytoskeleton are important protein networks that govern cellular behavior and are connected together by the linker of nucleoskeleton and cytoskeleton (LINC) complex. Mutations in LINC complex components may be relevant to cancer, but how cell-level changes might translate into tissue-level malignancy is unclear. We used glandular epithelial cells in a three-dimensional culture model to investigate the effect of perturbations of the LINC complex on higher-order cellular architecture. We show that inducible LINC complex disruption in human mammary epithelial MCF-10A cells and canine kidney epithelial MDCK II cells mechanically destabilizes the acinus. Lumenal collapse occurs because the acinus is unstable to increased mechanical tension that is caused by up-regulation of Rho kinase dependent non-muscle myosin II

Corresponding authors email addresses: Tanmay P. Lele: tlele@che.ufl.edu, Daniel E. Conway: dconway@vcu.edu.

*Co-corresponding authors: Lele and Conway

Author Contributions

Q.Z., V.N., K.L.M., C.S.O., R.H.A., B.K. designed, performed experiments and interpreted results. K.J.R., T.E.A., G.G.G., R.B.D., D.E.C., T.P.L., K.B.D., J.I.D., and S.A. designed experiments and interpreted results. T.P.L. wrote the manuscript with support from Q.Z., V.N., C.S.O., K.J.R., T.E.A., G.G.G., R.B.D., D.E.C.

#Authors contributed equally to this work.

†Lead Contact: Tanmay P. Lele

Declaration of Interests

The authors declare no competing interests.

motor activity. These findings provide a potential mechanistic explanation for how disruption of LINC complex may contribute to a loss of tissue structure in glandular epithelia.

Blurb:

Zhang *et al.* describe a functional role for the LINC complex, which links the nucleus to the cytoskeleton, in acinar development. Disrupting the LINC complex causes the development of acini with occluded lumens, and upregulates myosin II regulatory light chain phosphorylation. This mechanically destabilizes the dynamically fluctuating acinus.

Keywords

nucleus; LINC complex; nuclear mechanics; acinar development; 3D culture

Introduction

The nucleoskeleton, which is comprised of Type V intermediate filament nuclear lamin proteins, confers mechanical stiffness to the nucleus and helps organize the genome [1]. The nucleoskeleton is connected to the cytoplasmic cytoskeleton by the LINC complex (linker of nucleoskeleton and cytoskeleton). The LINC complex transmits mechanical forces generated in the cytoskeleton to the nucleus, which positions the nucleus in cells and tissues, and enables crucial functions like the establishment of cell polarity, cell migration, cell mechanosensing and gene expression [2–10].

The LINC complex spans the inner and outer nuclear membranes. It is composed of an inner membrane protein containing the Sad1 and UNC-84 (SUN) domain, and an outer membrane protein containing the Klarsicht, ANC-1, and Syne homology (KASH) domain. The SUN and KASH domains bind to each other in the perinuclear space [11–14]. The mammalian genome encodes five SUN proteins, which are anchored in the inner nuclear membrane and several of these interact with lamin A/C and emerin. [2, 11, 15]. By contrast, the mammalian genome encodes six KASH proteins (nesprins 1–4, KASH5 and LRMP) [3, 16]. The cytoplasmic domain of nesprins interact directly or indirectly with actin filaments (nesprin-1 and nesprin-2), microtubules (nesprin-1, nesprin-2, and nesprin-4, and KASH5) and intermediate filaments [6, 7, 12, 13, 17–20].

Emerging evidence suggests that alterations to LINC complex proteins may contribute to the development of pathologies. Complete double knockout (DKO) of nesprin-1 and nesprin-2, as well as SUN1 and SUN2, is lethal in mice [21, 22]. Loss of nesprin-4 results in deafness in humans [23]; mutations in *SYNE1*, which encodes nesprin-1, causes cerebellar ataxia [24, 25], and alterations in LINC complex proteins are associated with Emery-Dreifuss muscular dystrophy [26, 27]. A recent study of 3,000 cancer genomes across nine cancer types identified mutations in the *SYNE-1* gene encoding nesprin-1 as “drivers” in the development of cancer [28]. LINC complex components SUN1, SUN2, and nesprin-2 are downregulated in breast cancer [29]. SYNE-1 and SYNE-2 genes can also be mutated or undergo gene amplification in breast cancers [29–31]. Glandular epithelia in the breast and other organs are characterized by tubular networks and acinar structures that contain hollow lumens.

Cancer development in glandular epithelia is generally characterized by a loss of tissue structure that includes blockage of glandular lumens [32, 33].

Here we examined the effect of LINC complex disruption on the development and maintenance of higher-order glandular epithelial cellular structures in three-dimensional culture. We focused on epithelial acini which model normal glandular epithelium *in vivo* [34–38]. We show that the LINC complex supports the maintenance of the glandular epithelia through its effects on non-muscle myosin II. Our results suggest a potential mechanistic role for alterations to the LINC complex in generating structural aberrations of glandular epithelial tissue.

Results

The role of the LINC complex in acinar development

To investigate the role of the LINC complex in epithelial acinar development, we first generated two MCF-10A breast epithelial cell lines in which the LINC complex could be disrupted in an inducible manner. We created one cell line that inducibly expresses SS-EGFPSUN1L-KDEL (abbreviated as SUN1L-KDEL). This construct binds to endogenous KASH domain proteins via a lumenal SUN domain but instead of a transmembrane tether to retain it at the NE, it has a KDEL retention motif to maintain it in the ER. Thus SUN1L-KDEL functionally depletes nesprins at the nuclear envelope thereby disrupting the LINC complex [11]. We also created an MCF-10A cell line that inducibly expresses SS-EGFP-KDEL (abbreviated as EGFPKDEL), to be used as a control. In both these cell lines, expression of recombinant proteins was induced by doxycycline. Consistently with our previously published observations with NIH 3T3 fibroblasts [39], perturbation of the LINC-complex by SUN1L-KDEL expression in MCF-10A cells in 3D culture led to loss of nesprin-2 and/or nesprin-4 (the antibody cross-reacts with human nesprins 2 and 4) from the nuclear envelope, as observed by immunofluorescence (Figure S1). Such loss was not observed in cells expressing EGFP-KDEL. Also, SUN1L-KDEL expression but not EGFP-KDEL expression caused a loss of nesprin-3 from the nuclear envelope in 3D MCF-10A culture (Figure S1C). These results demonstrate successful, inducible disruption of the LINC complex in MCF-10A cells in 3D culture.

To examine the effect of LINC disruption on acinar formation, we induced the expression of EGFP-KDEL or SUN1L-KDEL in MCF-10A cells for 48 h and cultured these cells in Matrigel™ over a period of several days. Acinar development by the two cell lines was markedly different. The cells producing EGFP-KDEL assembled acini that were almost spherical (Figure 1A), with a clearly visible lumen. Over the same time period, cells producing SUN1L-KDEL also assembled almost spherical structures, but around 80% of these spheres lacked a lumen (Figure 1B). We confirmed that these effects were not due to differences in the expression levels of EGFP-KDEL and SUN1L-KDEL (Figure S1D). These observations indicate that an intact LINC complex is required for the development of MCF-10A acini with organized lumens.

We next examined the generality of these findings by using alternative approaches to disrupt the LINC complex. We expressed the KASH2 domain from nesprin-2, which has been

shown to disrupt the LINC complex by competitively binding to SUN1/2 [20, 40, 41]. Similar to the observations with EGFP-SUN1L-KDEL expressing cells, EGFP-KASH2 expression in MCF-10A cells caused more than a two-fold decrease in the number of acini with lumen but did not prevent the formation of spherical structures (Figure 1A and 1B). Expression of EGFP or the KASH domain lacking the luminal domain (EGFP-KASH2 DL), which does not disrupt the LINC complex [40, 42], did not affect lumen formation (Figure 1A and 1B). These results indicate that the observed lack of lumen in MCF-10A acini is caused by LINC complex disruption and independent of the method used for the disruption.

To check whether the observed LINC complex requirement for normal acinar development is cell-type specific, we engineered MDCK II cells to inducibly express mCherry-KASH1 (abbreviated as KASH1; the KASH1 domain was from nesprin-1). KASH1 production was first induced in these cells, and this was followed by a 7-d culture in Matrigel™ to stimulate acinar development. KASH1 expression was confirmed to cause a loss of nesprin-1 and nesprin-2 from the nuclear envelope as observed by immunofluorescence in both 2D and 3D cultures (Figure. S2). As a control, we engineered MDCK II cells to inducibly express mCherry-KASH1ΔPPPL (abbreviated as KASH1ΔPPPL) which does not interact with SUN proteins [40, 43]; we confirmed that this construct does not displace nesprin-2 from the nuclear envelope in 2D and 3D cultures (Figure. S2). In KASH1 expressing cells, we observed the formation of assembled structures that displayed multiple lumens, with cortical F-actin present near the curved surface of the lumens and between cells (Figure 1C). In some cases, acini were observed to be completely occluded. Such phenotypes were absent in the uninduced control and in the KASH1ΔPPPL control. Also, effects on acini were not attributable to differences in the expression levels of KASH1ΔPPPL and KASH1 constructs (Figure. S2C).

Collectively, these data indicated that LINC complex disruption, regardless of the disruption method, the cell model and species used (human vs. canine), results in abnormal acinar development.

The role of the LINC complex in acinar maintenance

The experiments described above indicated that the disruption of the LINC complex affects normal acinar development. We hence asked whether the LINC complex was required to maintain lumens in normally developed acini. We allowed MDCK II cells to develop acini for 7 d, at which time the cells formed spherical acini with a well-defined lumen (Figure 2A). We then induced the expression of KASH1 or KASH1ΔPPPL in these cells with doxycycline at the end of day 7. The KASH1 acini became occluded upon doxycycline treatment after a relatively short time (1–2 d) unlike KASH1ΔPPPL acini (Figure 2A and 2B). These observations suggest that LINC complex disruption can destabilize existing acini, indicating that LINC complex alterations in tissue might lead to loss of tissue structure. Upon induction of SUN1L-KDEL expression by doxycycline treatment, MCF-10A acini also became similarly occluded in 2 days (Figure 2C and 2D).

To gain insight into the mechanism by which LINC complex disruption might cause occlusion of the pre-existing lumen in normally formed acini, we first characterized the acinar and nuclear geometric changes induced by DN-KASH expression (Figure S3). We

observed no significant changes in the overall acinar geometry with DN-KASH expression. Additionally, changes in nuclear geometry were not consistent between MCF-10A and MDCK II cells, suggesting that other mechanisms were responsible for the destabilization of the acinar structure. Next, we used live-cell imaging to understand acinar dynamics and how those dynamics change with LINC complex disruption. Figure 3 shows a typical example of an acinus formed by MDCK II KASH1ΔPPPL cells (see Video S1), with a fluctuating lumenal shape and acinar boundary. In these acini, the local regions of the acinar surface appeared to thicken and thin out constantly over a time period of a few hours. The thinned parts eventually recovered to thicken again. Elsewhere, parts of the surface transiently thickened. Such thinning and thickening appeared to proceed randomly and relatively quickly).

We then examined the acinar dynamics in pre-formed acini that were treated with doxycycline to induce the expression of KASH1. Upon doxycycline treatment, the acini were immediately transferred onto the microscope stage so that acini could be imaged as the levels of KASH1 increased with time. Unlike control acini, shape fluctuations of the KASH1-expressing acinus were not stable. Once the acinar boundary began to thin, the thin area continued to thin out; the opposite was also true: thickened areas continued to thicken (Figure 3). Eventually, the thick boundary moved inward and met the thin boundary, to collapse the lumen (after 16 h of induction; see Videos S2 & S3). The entire process, from the first observation of thinning to lumenal collapse, occurred rapidly within approximately 3 h, resulting in the formation of a solid mass of cells. Hence, while normal acini quickly recover from fluctuations of cells forming the acinar boundary, LINC complex-disrupted acinar lumens collapsed irreversibly. The collapse was not always complete, but was observed also in parts of the acinus, which caused partial occlusions. The partial occlusions similarly were preceded by local thinning of the acinar surface and rapid local collapse (see Videos S4 for an example). These data suggest that LINC complex-disrupted acini may be mechanically unstable.

The involvement of non-muscle myosin (NMMII) in loss of acinar architecture mediated by LINC complex disruption

We next explored the possible causes of the observed lumenal collapse. Because actomyosin forces have been shown to play an important role in the development and maintenance of tissues [44–46], particularly in the context of glandular acini [33, 47–50], we asked whether non-muscle myosin II (NMMII) was involved in the lumenal collapse after LINC complex disruption. The time scale (approximately ~1 h) of fluctuations in the acinar shape, i.e., local cell thinning and thickening, also supported the possibility that the fluctuations and subsequent collapse were likely associated with the NMMII-generated contractile forces, which are known to operate on such time scales in epithelia [51]. While control acini were clearly stable to the presence of these fluctuations (Video S1), it is possible that upon LINC complex disruption, the acini become unstable because of an increase in the magnitude of actomyosin contractile forces. To test this possibility, we quantified the effect of LINC complex disruption on myosin regulatory light chain phosphorylation (pMLC) which regulates myosin ATPase activity and hence actomyosin tension in MDCK II acini [52]. LINC disruption did not affect pMLC levels probed with an anti-myosin light chain

(phospho S20) antibody in cells harvested from two-dimensional culture (Figure 4A and 4C, slight increase but with no statistical difference). We confirmed that small molecule perturbations of NMMII activity had the expected effects: treatment with the ROCK inhibitor Y27632 reduced pMLC levels, treatment with Rho activator II, a small molecule agonist of Rho, increased pMLC levels, while treatment with blebbistatin, an NMMII inhibitor, had no effect consistent with previous reports [53–55] (Figure 4A and 4C). Interestingly, there was a statistically significant increase in pMLC levels in LINC disrupted cells harvested from acini formed in three-dimensional culture (Figure 4B and 4C). These data support the possibility that LINC complex-disrupted acinar lumens collapse due to an increase in NMMII-mediated tension. As revealed by immunostaining, pMLC did not localize to F-actin bundles in the acinus consistent with previous reports [56]. This suggests that in acini, NMMII likely generates contractile forces in disordered gel-like F-actin networks that pervade cytoplasmic space [57]. Furthermore, neither LINC disruption nor treatment with NMMII agonists had any discernible effects on the spatial distribution of pMLC in acini (Figure. S4).

To test the possibility that increased NMMII contractility can destabilize the spherical acinus and induce lumenal occlusion, we treated MDCK II acini with calyculin A. Calyculin A inhibits myosin light chain phosphatase and increases pMLC levels in cells, increasing NMMII-mediated tension [58–60]. Calyculin A treatment induced a similar dynamic mode of lumenal collapse as was observed for LINC complex-disrupted acini. Specifically, local thinning and simultaneous thickening at other acinar surfaces (sometimes located at the opposite acinar pole) leading to lumenal collapse were observed (Figure 4D and Videos S5 & S6). The time scale for collapse from the initial thinning and thickening event was approximately 2–4 h, similar to the time scale observed in lumenal collapse upon LINC disruption (Figure 3 and Videos S2 & 3). Further, lumenal collapse was consistently preceded by a localized thinning/thickening, which was a reproducible consequence of LINC complex disruption and calyculin A treatment (Figure 4D). We also treated acini with Rho activator II and found similar reproducible collapse of acini after 2–4 h (Figure 4D; Video S7; Figure 4A shows that Rho activator II treatment increased pMLC levels). Furthermore, acinar collapse was dependent on the dose of Rho activator II (Figure 4E). Treatment of acini with lower doses of Rho activator II at which acini did not collapse, still caused a significant increase in acinar fluctuations (Figure 4F) relative to the DMSO treated control (Figure 4F). Treatment with the Y27632 and blebbistatin, on the other hand, reduced the fluctuations in the local thickness of the acinus (Figure 4F, Videos S8 & 9), suggesting that acinar fluctuations are NMMII dependent. Collectively, these findings support the plausibility of lumenal collapse upon LINC disruption being a type of mechanical instability triggered by increased acinar fluctuations caused by an increase in NMMII-mediated contractile forces.

Motivated by these observations, we asked whether inhibiting NMMII would rescue lumenal collapse in acini in which the LINC complex was disrupted. When blebbistatin, an NMMII inhibitor, was included in the acinar culture medium (on day 4 of culture), lumen formation by KASH1-producing MDCK II cells was rescued (Figure 5A and corresponding plot in 5B, acinar development). Likewise, the presence of blebbistatin prevented LINC complex disruption from altering pre-formed acini (Figure 5A and corresponding plot in 5B, acinar

maintenance). These experiments suggest that actomyosin forces may drive lumenal collapse in LINC complex-disrupted MDCK II acini.

To determine whether the up-regulation in NMMII motor activity observed in cells with LINC complex disruption was ROCK-dependent, we treated the induced MDCK II acini (acini where the LINC complex was disrupted) with Y-27632. Including Y-27632 on day 4 of culture prevented lumenal blockage during acinar development (Figure 6A, 6B). Similarly, providing the inhibitor together with doxycycline on day 7 prevented lumenal blockage in preformed MDCK II acini as well as in preformed MCF-10A acini (Figure 6A, 6B). Further, live imaging of MDCK II acinar revealed that Y-27632 treatment of induced acini caused an increase in the size of the LINC disrupted acinus over a 20 h period which was not observed in the KASH1ΔPPPL control nor in the uninduced control (Figure 6C. and 6D). As noted above, Y-27632 treatment eliminated the fluctuations in acinar thickness (Figure 6C) that were observed in control acini and also caused acinar thinning (Figure 6C, 6D and Video S10). Collectively, these observations demonstrated that the destabilization of lumenal shape brought about by LINC complex disruption requires ROCK-regulated NMMII light chain phosphorylation.

LINC complex disruption alters acinar mechanics and promotes cell division inside the filled lumen

Changes to multicellular tissue architecture, particularly lumenal filling, can cause significant changes to the mechanical properties of the acinus, which cause downstream changes in cell function and gene expression and potentially promote cellular malignancy [32, 61]. We therefore performed mechanical measurements in which a glass hemisphere was pressed against isolated acini assembled by MDCK II cells and the applied force was recorded, with simultaneous fluorescence imaging of the cells (Figure 7A). When the applied forces exceeded background noise levels, the acini were observed to flatten out. Further increase in the applied force resulted in structural collapse of the acini through the formation of cellular blebs and/or bursting of cells. Pinpointing the applied pressure at which such failure was first observed, we found that acini with disrupted LINC complexes failed at higher applied pressures than cells with intact LINC complexes (Figure 7A). Such increased resistance to rupture of LINC disrupted acini is consistent with the presence of filled lumens. We also performed these experiments on LINC-disrupted acini treated with Y-27632, and as expected, Y-27632 treatment restored the failure pressure of LINC disrupted acini to control levels (Figure 7A). These results support the concept that NMMII-mediated lumenal filling in LINC disrupted acini may alter the mechanical micro-environment of cells [49], and could potentially give rise to further changes in cellular function.

Consistent with the observed changes in acinar mechanics, E-cadherin containing cell-cell adhesions were observed both in the peripheral regions of acini, as well as in between cells inside the lumen (Figure 7B), and these overlapped with F-actin bundle formation. Given that E-cadherin linkages transmit actomyosin force between cells, these results show that post lumenal collapse, cells retain cell-cell contacts and are integrated mechanically at least to some extent throughout the acinus.

In normal acini, cells in the lumen undergo apoptosis, while cells divide along the acinar periphery. Loss of tissue structure and abnormal micro-environmental mechanics can lead to loss of confinement of mitosis to the peripheral regions of acini. To test the possibility that cell division may be impacted by LINC complex disruption, we examined the mitotic spindle by imaging the microtubule network and DNA in MDCK II acini (Figure 7C). Cell division could be observed throughout the filled lumens, clearly indicating that LINC complex disruption promoted subsequent unconstrained cell division in the collapsed lumenal space. Mechanically induced changes to multicellular architecture upon LINC complex disruption can cause downstream aberrations in cell proliferation.

Nuclei in 3D acini are relatively uniformly positioned such that the nuclear-Golgi axis is oriented toward the lumen [34]. As the LINC complex is known to control nuclear position [17], we examined the effect of LINC disruption on the orientation of the nuclear-Golgi axis relative to the radial direction in MCF-10A cells. The nuclear-Golgi axis oriented early during acinar development (Figure 7D) toward the center of the initial cluster of dividing cells, for both control as well as LINC disrupted cells (Day 3, Figure 7D), and continued to be directed toward the lumen during subsequent development (day 4 through day 8, Figure 7D, and plot). Additionally, we probed the spatial localization of the polarity marker gp135 in MDCK II acini. Gp135 is localized to the apical surface of the MDCKII acinus in control acini. Gp135 continued to be localized to the luminal surface in partially collapsed acini at 24 h of LINC disruption (Figure 7E and plot). These results suggest that lumenal collapse caused by LINC disruption is not preceded by changes to cell polarity.

Discussion

Available evidence implicates the LINC complex in cancer development, but little is known about the underlying molecular and mechanistic processes. Specifically, a convincing explanation for how cell-level changes translate into tissue-level malignancy is lacking, in part because of the limited insight provided by the two-dimensional cell culture used in most studies. In this study, we used glandular epithelial cells in a three-dimensional culture model to investigate the effect of LINC disruption on higher-order cellular architecture. We showed that inducible disruption of the LINC complex results in the development of aberrant acini, i.e., acini that lack lumen or display multiple lumens. The aberrant phenotypes were not specific to the method used for LINC complex disruption and were not restricted to single cell type or species. Further, the rapid lumenal collapse occurred as a result of increased NMMII activity, mediated by ROCK, affecting actomyosin forces.

Assembling acini in stiff extracellular matrices results in lumenal filling, while acini assembled in soft matrices assemble normal lumens [33], and inhibiting NMMII activity rescues lumen formation in stiff extracellular matrices. These results, together with our observations, suggest that lumenal filling will occur upon increase in actomyosin tension, independent of the type of perturbations. Our dynamic imaging experiments of the process of lumenal collapse suggest that increased cellular actomyosin tension due to treatment with calyculin A or Rho activator II or due to LINC complex disruption caused lumenal collapse through an inward movement of thickening acinar boundaries toward thinning acinar surfaces (Figures 3 and 4). Conversely, inhibiting cellular actomyosin tension caused the

lumen to increase in size with thinning of the cellular boundaries (Figure 6C & 6D). Collectively, these results together with previous studies, suggest that the acinus is mechanically unstable to enhanced cellular actomyosin activity. The observed expansion and thinning of the acinus upon inhibition of cellular actomyosin tension, and compression and collapse of the acinus upon increase in actomyosin tension are consistent with the simple mechanical model illustrated in Figure 7F. A normal acinus reflects a state of mechanical equilibrium where the surface tension T of the spherical monolayer, assumed to be generated by actomyosin contraction, balances the lumenal pressure P. We speculate that P is maintained by a physiological process, such as ion transport, to maintain a higher osmotic pressure inside the lumen than outside it. Based on the Law of Laplace, the stress balance may be described as

$$2T/R = P \quad (1)$$

where R is the radius of curvature of the lumen. If the surface tension and pressure are maintained by cellular processes independent of the size of the acinus, then the mechanical equilibrium expressed in Equation 1 is unstable. That is, an increase in T (such that $2T/R > P$) will cause the acinus to compress and thus decrease its radius. However, this reduces the radius of curvature, which, according to equation 1, would further move the system away from a mechanical equilibrium and, ultimately, towards lumenal collapse. On the other hand, a decrease in T, such that $2T/R < P$ will cause the acinus to continually expand until the stretched cells in the monolayer finally reach a mechanical limit to further thinning. Establishing and sustaining such an unstable mechanical equilibrium would require a control mechanism (which requires further investigation) to regulate T and/or P in response to actomyosin fluctuations.

Disruption of the LINC complex can alter cell mechanotransduction [62, 63], mechanosensitive gene expression [64], nuclear body dynamics [65, 66], cell migration [67], nuclear positioning [5, 17, 68–71], the assembly of the actomyosin cytoskeleton [5, 72–74], and the mechanical properties of the nucleus [39]. Our results add to this literature, by showing that mechanical continuity between the nucleus and the cytoskeleton is required for maintaining three-dimensional tissue architecture and mechanics. The molecular pathways upstream of ROCK/NMMII that are regulated by the LINC complex during acinar morphogenesis are presently unclear but are likely to be complex based on emerging evidence about the interplay of LINC complex components with the RhoA pathway. For example, there is evidence that the LINC complex protein SUN1 antagonizes RhoA activity while Sun2 promotes it [75]. Further, LINC complex proteins can also impact gene expression independently of incorporation into the LINC complex [76]. These pathways require further investigation. The model in Figure 7F suggests that molecular interactions between the LINC complex and ROCK-dependent NMMII ATPase activity are critical for acinar structural stability, and LINC complex disruption destabilizes the acinus by causing hyper-contractility.

In addition to collapse of pre-formed acini upon LINC complex disruption, our data shows that the process of acinar morphogenesis itself also becomes abnormal resulting in assembly

of acini that lack a lumen. Including inhibitors like blebbistatin or Y27632 at day 4 did prevent the formation of occluded acini by day 7 during MDCK II acinar development (Figure 5 and 6A). However, a limitation of our study is that the process of acinar development itself is significantly more complex involving cell division and apoptosis. The mechanism by which LINC complex disruption impacts the development of acini may involve more than alterations to cellular actomyosin tension alone, particularly in MCF-10A cells which develop over many days. Another limitation of our study is that our approach relied on dominant negative proteins which displace all nesprin proteins from the LINC complex. Given that nesprin-2 has been shown to be downregulated in cancer, and mutations identified primarily in nesprin-1 and nesprin-2 in cancer, studies that focus on the impact of specific nesprin proteins will be required to establish a more direct connection with cancer. Our working hypothesis is that alterations to nesprin proteins likely disrupt the LINC complex in a similar manner as demonstrated here. Finally, the extent to which results from the model systems studied here are applicable to actual cancer development is unclear and will require further investigation with animal models.

Collectively, our findings add weight to the concept that physical forces play a crucial role in the development and maintenance of tissues [44–46], particularly in the context of glandular acini [33, 47–50, 77]. The presented findings should provide impetus for studies of the LINC complex in the context of cancer progression.

STAR Methods

LEAD CONTACT AND MATERIALS AVAILABILITY

Plasmids generated in this study have been deposited to Addgene (mcherry-DNKASH, 125553; pinducer20-mcherry-DNKASH1 125554; pinducer20-mcherry_DNKASH1ΔPPPL, 129280). Further information and requests for resources and reagents (including stable cell lines and other plasmids) should be directed to and will be fulfilled by the Lead Contact, Tanmay P. Lele (tlele@che.ufl.edu).

EXPERIMENTAL MODEL AND SUBJECT DETAILS

Stable cell lines—To generate a system for doxycycline-inducible LINC complex disruption in MCF-10A cells, the cells were transduced using the pRetroX-Tet-On-Advanced system (Clontech) and then incubated in DMEM/10% FCS containing 0.5 mg/ml G418 to select for cells that stably express the rtTA-Advanced protein. The cells were subsequently transduced using pRetroX-Tight.puro (Clontech), followed by a selection on medium containing 1 mg/ml puromycin. Plasmid pRetroX.Tight.puro harbored either sequences encoding SS-EGFP-SUN1L-KDEL (SUN1LKDEL) or SS-EGFP-KDEL (EGFP-KDEL) [11]; in the latter, the EGFP sequence alone was targeted to and retained in the ER lumen as a control. After puromycin selection, expression of the SS-EGFP-SUN1L-KDEL or SS-EGFP-KDEL was induced with 1 μg/ml doxycycline for 18 h, and FACS-sorted to select cells that expressed EGFP protein. These cells were subsequently screened by immunofluorescence with or without 1 μg/ml doxycycline for 18 h to ensure that the cells were only expressing the fusion proteins upon induction of expression with doxycycline. To generate the constructs for MCF-10A EGFP-KASH2 and EGFP-KASHΔL cells. pLVX-

puro-EGFP-C2 vector was derived from pLVX-puro vector (Clontech) by inserting EGFP-MCS sequence. cDNAs for human nesprin-2 KASH (6829–6907 aa) and KASHΔL (6829–6884 aa) were previously described [40] and were inserted into pLVX-puro-EGFP-C2 vector with BamHI and NotI restriction sites.

To create a dominant-negative KASH1 (DN-KASH1) peptide (originally developed by Lombardi *et al.* [78]) mCherry dominant negative (DN)-KASH1 protein was prepared by cloning the sequence encoding the KASH domain from human nesprin-1 (synthesized by Gene Art, Thermo Fisher) into pmCherry-C1 (Clontech). Similarly, to create a control KASH1 peptide which could not interact with SUN proteins, the last 4 amino acids of KASH1 (Pro-Pro-Pro-Leu) were deleted from this construct (referred to as KASH1ΔPPPL) [43]. To develop an inducible lentivirus, the sequences encoding mCherry-DN-KASH1 and mCherry-DN-KASH1ΔPPPL were each inserted into pinducer20 (gift from Stephen Elledge; Addgene plasmid #44012) [79]. Lentivirus was generated using HEK 293 cells (ATCC) and standard second-generation packaging plasmids[80]. After lentiviral infection [80], MDCK II cells were selected using G418, and then induced to express mCherry-KASH1 with 100 ng/ml doxycycline. Cells expressing high levels of mCherry-KASH1 or mCherry-KASH1ΔPPPL were sorted by flow cytometry and were clonally expanded.

Cell culture and drug treatment—Cells were maintained at 37°C in a humidified 5% CO_2 environment. Human breast epithelial cells (MCF-10A from ATCC) were maintained in DMEM/F12 medium (Invitrogen) supplemented with 20 ng/ml epidermal growth factor (EGF, Peprotech), 0.5 mg/ml hydrocortisone (Sigma), 100 ng/ml cholera toxin (Sigma), 100 μg/ml insulin (Sigma), 1% v/v penicillin-streptomycin mix (Pen-Strep, Invitrogen), and 5% v/v horse serum (Invitrogen) [34]. MDCK II cells (gift of Jennifer Lippincott-Schwartz) were cultured in DMEM medium with 4.5 g/l glucose (Mediatech Cellgro), supplemented with 10% v/v donor bovine serum (DBS, Gibco). To induce acinar formation in MCF-10A cells, cells were trypsinized and re-suspended in assay medium consisting of DMEM/F12 supplemented with 0.5 mg/ml hydrocortisone, 100 ng/ml cholera toxin, 100 μg/ml insulin, 1% v/v penicillin-streptomycin mix (Pen-Strep) and 2 % v/v horse serum [34]. Cells were next seeded in the assay medium supplemented further with 5 ng/ml EGF and 2% v/v Matrigel™ on growth factor reduced (GFR) Matrigel™ (Corning)-coated 8-well Nunc Lab-Tek chamber slides (5000 cells/well) as previously described [34]. To coat an 8-well Nunc Lab-Tek chamber slide with Matrigel™, 40 or 45 μl of Matrigel™ was spread evenly on each well of 8-well chamber slide. Then the chamber slide was kept in the incubator for at least 30 min until the gels were solidified. For studying the effect of LINC complex disruption on MCF-10A acinar development, MCF-10A cells were induced to express specific control proteins or dominant negative proteins by treatment with 1 mg/ml doxycycline for 48 h before seeding into Matrigel™. To induce acinar formation in MDCK II cells, cells were cultured in MDCK II growth medium supplemented with 2% v/v Matrigel™, on GFR Matrigel™ (Corning)-coated 8-well Nunc Lab-Tek chamber slide system (5000 cells/well) for 7 d. For studying the effect of LINC complex disruption on MDCK II acinar development, cells were induced to express dominant negative mCherry-KASH1 by treatment with 1 mg/ml doxycycline for 24 h. In acinar maintenance experiments, MCF-10A or MDCK II cells were allowed to form acini and then treated with

1 μg/ml doxycycline for indicated times. For myosin inhibition, Y27632 (EMD Millipore) at final concentrations of 40 μM and blebbistatin (EMD Millipore) at 50 μM were used. For increasing myosin activity, calyculin A (Cell Signaling Technology) at a final concentration of 5nM and Rho activator II (Cytoskeleton Inc) at final concentrations of 1 μg/ml, 2.5 μg/ml and 5 μg/ml were used.

METHOD DETAILS

Immunostaining—Acini were immunostained using the protocol of Debnath *et al.* [34]. To immunostain acini in 3D Matrigel™, cells were first fixed with 2% paraformaldehyde for 20 min at room temperature. Then the fixed acini were incubated in permeabilization buffer (0.5% Triton X-100 in PBS) for 30 min at room temperature followed by another 45 min incubation with IF buffer (130 mM NaCl; 7 mM Na_2HPO_4; 3.5 mM NaH_2PO_4; 7.7 mM NaN_3; 0.1% BSA; 0.2% Triton X-100; 0.05% Tween-20) supplemented with 10% goat serum. Acini were incubated with primary antibody rabbit anti-GM130 (Cell Signaling Technology, working dilution 1:2000), mouse anti-GP 135,EMD Millipore, clone 3F2:D8, concentration: 0.5 mg/ml, working dilution 1: 250), rabbit anti-Nesprin 2/4 (peptide antigen KKAELEWDPAGDIGGLGPLGQ; YenZyme, working dilution 1:200, described in [39], rabbit anti-Nesprin 3 (Sigma, working dilution 1:100), rabbit anti-Nesprin 2 (described in an earlier study [40], dilution 1:200), mouse anti-Nesprin 1 (EMD Millipore MANNES1A clone 7A12, dilution 1:50), mouse anti-alpha tubulin (Sigma, working dilution 1:250), rabbit anti-ECadherin (24E10) (Cell Signaling Technology, working dilution 1:200) and rabbit anti-myosin light chain (phospho S20) (Abcam, working dilution 1:100, previously validated for MDCK II cells [81]) overnight at 4°C. The samples were then washed with PBS and incubated with secondary antibodies Alexa Fluor 594 goat anti-rabbit antibody, Alexa Fluor 647 chicken anti-rabbit antibody, Alexa Fluor 647 donkey anti-mouse antibody and Alexa Fluor 488 goat anti-rabbit antibody was used for 2 hrs at room temperature (Invitrogen, working dilution 1:200). Phalloidin conjugated to a fluorophore (Alexa Fluor 488, 594, or 647; Life Technologies) was used to stain F-actin. The nucleus was stained with Hoechst 33342 (Life Technologies/Invitrogen) or DAPI stain (Vector Laboratories).

Mechanical indentation assay—Indentation experiments were performed using a custom micro-indenter consisting of a sapphire probe with a 1.6-mm curvature radius fastened to a double-leaf cantilever [82]. The cantilever was mounted to a piezoelectric stage (Physik Instrumente P-622.ZCL). Normal forces were calculated by measuring the deflection of the cantilever using a linear displacement capacitance probe (Lion Precision C5R-0.8 sensor). Acini were isolated from Matrigel™ (following steps described in Lee *et al.*, [83]) and deposited on glass-bottom petri dishes (Cell Vis) coated with 0.01% poly-L-lysine (Sigma). To isolate acini, acini were first washed once with PBS at 4°C and then incubated with PBS at 4°C supplemented with 5 mM EDTA, 1 mM $NaVO_4$, 1.5 mM NaF until most of the gels were dissolved. This was followed by 15 min centrifugation at 125 g and 4°C. The pellet was next rinsed with 4°C PBS and then centrifuged again at 4°C, 125 g for 15 min. To check the viability of acini, isolated acini were incubated with calcein AM (Invitrogen, 1:2000). To avoid adhesion to cells, the indenter probe was coated with 0.1 wt% pluronic F-127. The micro-indenter was mounted above a laser-scanning confocal microscope (Nikon C2) to perform real-time imaging of the acini during indentation.

Indentation measurements were performed at an indentation speed of 0.1 μm/s to a maximum load of 50 μN.

Determination of spindle-angle orientation—The spindle angle was measured as the acute angle between the line joining the two poles of the mitotic spindle, and the line joining the mid-point of the spindle line and the centroid of the apical domain. The measurements were performed in Image J [84].

Western blotting—For assaying cells in 2D culture, cells were washed with cold phosphate-buffered saline (PBS) and lysed in lysis buffer (50 mM Tris-HCl pH 7.2, 1% (w/v) Triton X-100, 500 mM NaCl, 10 mM $MgCl_2$ and 0.1% v/v SDS) supplemented with 1% v/v protease inhibitor (Cytoskeleton Inc.) on ice. Cells were then scraped from the dish and centrifuged at 10,000 rpm (Eppendorf, 5415R) for 5 mins at 4°C. The supernatant was collected, s nap-frozen in liquid nitrogen, and stored at – 80°C. Total protein concentration was determined us ing Precision Red advance protein kit (Cytoskeleton, Inc.). For cells cultured in 3D Matrigel™, we used previously published protocols from the Brugge lab [34, 85]. Briefly, cells were washed with cold PBS and lysed in RIPA buffer (Alfa Aesar) supplemented with 1% protease inhibitor for 15 mins at 4°C. The cell, Matrigel™ and lysis buffer mixture was pulled through 27-gauge needle 3 times and allowed to sit at 4°C for 15 mins. The lysate was spun for 15 mins at 4°C at 13200 rpm (Eppendorf, 5415R). The supernatant was collected and snap-frozen in liquid nitrogen. The CytoTox 96 kit (Promega) was used to detect lactate dehydrogenase (LDH) levels, which was used to normalize lysate concentrations for equal loading. Expression levels of individual proteins were quantified using the WES™ system (Protein Simple) and the 12–230 kDa WES kit (SM-W004), according to manufacturer's instruction. The primary antibodies used were rabbit anti-p(myosin) (ab 2480, Abcam) against phosphorylated myosin (S20) that have been previously validated for MDCK II cells [81] and mouse anti-GAPDH antibodies (NB300–328SS, Novus Biologicals). The secondary antibodies used were from the WES™ detection kit, anti-rabbit (042–208) and anti-mouse antibodies (042–205) and used as per manufacturer's instructions. Data analysis was performed using ProteinSimple Compass software. The total intensity for each band was computed as the area under each peak (computed automatically by the software). Next, the total intensity for each band was divided by the total intensity of the corresponding GAPDH band. Next, for a given blot, the data normalized as above in each lane was further normalized to the normalized data in a reference lane.

Imaging and analysis—Fluorescence imaging of cells/acini was performed using a Nikon A1+ confocal microscope or Nikon epifluorescent microscope equipped with a 60× oil immersion objective with 1.4 N.A.,40× oil immersion objective with 1.3 N.A., 40× water immersion objective with 1.15 N.A., or 10× objective with 0.3 N.A. (all from Nikon). Epifluorescence imaging made use of a CCD camera (CoolSNAP, Photometrics), while confocal images were captured with DU4 detector. For all live-acinar imaging, the cells were maintained in an environmental chamber (In Vivo Scientific) at 37°C and 5% CO_2. Time-lapse imaging of acini was performed using a 20× objective, 0.75 N.A. or 40× objective, 0.6 N.A. (Nikon). The correction collar of each objective was adjusted based on the

manufacture's suggestion for different cover glasses. The filter cube used for live cell imaging was 540/20 excitation and 600/25 emission.

QUANTIFICATION AND STATISTICAL ANALYSIS

Matlab was used to analyze the mean squared fluctuations reported in Figure 4F. Student's t-test was used to detect the statistical difference between MCF-10A groups. Bonferroni correction was used if multiple comparisons were performed. One-way ANOVA followed by Tukey (*HSD*) test was used to compare different phenotypes formed by MDCK II cells using the R software [86] (Figure 1D, 2B and S2D). Data are presented as mean ± SEM. Detailed experimental design (replication and sample sizes) and statistical information can be found in Figure Legends.

DATA AND CODE AVAILABILITY

All data and code supporting the findings of this study are available from the corresponding authors upon request.

Supplementary Material

Refer to Web version on PubMed Central for supplementary material.

Acknowledgements

This work was supported by the National Institutes of Health (grants R01 EB014869 to T.P.L.; R35 GM119617 to D.E.C.; GM099481 to G.G.G.; and 1F32CA221320–01 to K.L.M.); and National Science Foundation (grants CAREER CMMI-1653299 to D.E.C.; and DMR-1352043 to T.E.A.). K.J.R. acknowledges the Imaging Core, and Flow Cytometry Core at Sanford Research, supported by NIH (grants P20GM103548 and P20GM103620). D.E.C. also acknowledges VCU Massey Cancer Center Biological Macromolecule Shared Resource supported by the National Institutes of Health (grant P30 CA016059). R.B.D's contribution was based upon work supported by (while serving at) the National Science Foundation.

References:

1. Davidson PM, and Lammerding J (2014). Broken nuclei--lamins, nuclear mechanics, and disease. Trends Cell Biol 24, 247–256. [PubMed: 24309562]
2. Chang W, Worman HJ, and Gundersen GG (2015). Accessorizing and anchoring the LINC complex for multifunctionality. J Cell Biol 208, 11–22. [PubMed: 25559183]
3. Alam S, Lovett DB, Dickinson RB, Roux KJ, and Lele TP (2014). Nuclear forces and cell mechanosensing. Prog Mol Biol Transl Sci 126, 205–215. [PubMed: 25081619]
4. Cho S, Irianto J, and Discher DE (2017). Mechanosensing by the nucleus: From pathways to scaling relationships. J Cell Biol 216, 305–315. [PubMed: 28043971]
5. Stewart RM, Zubek AE, Rosowski KA, Schreiner SM, Horsley V, and King MC (2015). Nuclear-cytoskeletal linkages facilitate cross talk between the nucleus and intercellular adhesions. J Cell Biol 209, 403–418. [PubMed: 25963820]
6. Isermann P, and Lammerding J (2013). Nuclear mechanics and mechanotransduction in health and disease. Curr Biol 23, R1113–1121. [PubMed: 24355792]
7. Uhler C, and Shivashankar GV (2017). Regulation of genome organization and gene expression by nuclear mechanotransduction. Nat Rev Mol Cell Biol 18, 717–727. [PubMed: 29044247]
8. Petrie RJ, Harlin HM, Korsak LI, and Yamada KM (2017). Activating the nuclear piston mechanism of 3D migration in tumor cells. J Cell Biol 216, 93–100. [PubMed: 27998990]
9. Petrie RJ, Koo H, and Yamada KM (2014). Generation of compartmentalized pressure by a nuclear piston governs cell motility in a 3D matrix. Science 345, 1062–1065. [PubMed: 25170155]

10. Alam S, Zhang Q, Prasad N, Li Y, Chamala S, Kuchibhotla R, Aggarwal V, Shrestha S, Jones A, Levy S, et al. (2016). The mammalian LINC complex regulates genome transcriptional responses to substrate rigidity. Scientific Reports 6, 38063. [PubMed: 27905489]
11. Crisp M, Liu Q, Roux K, Rattner JB, Shanahan C, Burke B, Stahl PD, and Hodzic D (2006). Coupling of the nucleus and cytoplasm: role of the LINC complex. J Cell Biol 172, 41–53. [PubMed: 16380439]
12. Starr DA, and Fridolfsson HN (2010). Interactions between nuclei and the cytoskeleton are mediated by SUN-KASH nuclear-envelope bridges. Annu Rev Cell Dev Biol 26, 421–444. [PubMed: 20507227]
13. Razafsky D, and Hodzic D (2009). Bringing KASH under the SUN: the many faces of nucleo-cytoskeletal connections. J Cell Biol 186, 461–472. [PubMed: 19687252]
14. Starr DA (2011). KASH and SUN proteins. Curr Biol 21, R414–415. [PubMed: 21640895]
15. Folker ES, Ostlund C, Luxton GW, Worman HJ, and Gundersen GG (2011). Lamin A variants that cause striated muscle disease are defective in anchoring transmembrane actin-associated nuclear lines for nuclear movement. Proc Natl Acad Sci U S A 108, 131–136. [PubMed: 21173262]
16. Kozono T, Tadahira K, Okumura W, Itai N, Tamura-Nakano M, Dohi T, Tonozuka T, and Nishikawa A (2018). Jaw1/LRMP has a role in maintaining nuclear shape via interaction with SUN proteins. J Biochem 164, 303–311. [PubMed: 29878215]
17. Gundersen GG, and Worman HJ (2013). Nuclear positioning. Cell 152, 1376–1389. [PubMed: 23498944]
18. Zhang Q, Skepper JN, Yang F, Davies JD, Hegyi L, Roberts RG, Weissberg PL, Ellis JA, and Shanahan CM (2001). Nesprins: a novel family of spectrin-repeat-containing proteins that localize to the nuclear membrane in multiple tissues. J Cell Sci 114, 4485–4498. [PubMed: 11792814]
19. Wilson MH, and Holzbaur EL (2015). Nesprins anchor kinesin-1 motors to the nucleus to drive nuclear distribution in muscle cells. Development 142, 218–228. [PubMed: 25516977]
20. Zhu R, Antoku S, and Gundersen GG (2017). Centrifugal Displacement of Nuclei Reveals Multiple LINC Complex Mechanisms for Homeostatic Nuclear Positioning. Curr Biol 27, 3097–3110.e3095. [PubMed: 28988861]
21. Lei K, Zhang X, Ding X, Guo X, Chen M, Zhu B, Xu T, Zhuang Y, Xu R, and Han M (2009). SUN1 and SUN2 play critical but partially redundant roles in anchoring nuclei in skeletal muscle cells in mice. Proc Natl Acad Sci U S A 106, 10207–10212. [PubMed: 19509342]
22. Zhang X, Xu R, Zhu B, Yang X, Ding X, Duan S, Xu T, Zhuang Y, and Han M (2007). Syne-1 and Syne-2 play crucial roles in myonuclear anchorage and motor neuron innervation. Development 134, 901–908. [PubMed: 17267447]
23. Horn HF, Brownstein Z, Lenz DR, Shivatzki S, Dror AA, Dagan-Rosenfeld O, Friedman LM, Roux KJ, Kozlov S, Jeang KT, et al. (2013). The LINC complex is essential for hearing. J Clin Invest 123, 740–750. [PubMed: 23348741]
24. Gros-Louis F, Dupré N, Dion P, Fox MA, Laurent S, Verreault S, Sanes JR, Bouchard JP, and Rouleau GA (2007). Mutations in SYNE1 lead to a newly discovered form of autosomal recessive cerebellar ataxia. Nat Genet 39, 80–85. [PubMed: 17159980]
25. Synofzik M, Smets K, Mallaret M, Di Bella D, Gallenmüller C, Baets J, Schulze M, Magri S, Sarto E, Mustafa M, et al. (2016). SYNE1 ataxia is a common recessive ataxia with major non-cerebellar features: a large multi-centre study. Brain 139, 1378–1393. [PubMed: 27086870]
26. Meinke P, Mattioli E, Haque F, Antoku S, Columbaro M, Straatman KR, Worman HJ, Gundersen GG, Lattanzi G, Wehnert M, et al. (2014). Muscular dystrophy-associated SUN1 and SUN2 variants disrupt nuclear-cytoskeletal connections and myonuclear organization. PLoS Genet 10, e1004605. [PubMed: 25210889]
27. Bonne G, and Quijano-Roy S (2013). Emery-Dreifuss muscular dystrophy, laminopathies, and other nuclear envelopathies. Handb Clin Neurol 113, 1367–1376. [PubMed: 23622360]
28. Cheng F, Liu C, Lin CC, Zhao J, Jia P, Li WH, and Zhao Z (2015). A Gene Gravity Model for the Evolution of Cancer Genomes: A Study of 3,000 Cancer Genomes across 9 Cancer Types. PLoS Comput Biol 11, e1004497. [PubMed: 26352260]

29. Matsumoto A, Hieda M, Yokoyama Y, Nishioka Y, Yoshidome K, Tsujimoto M, and Matsuura N (2015). Global loss of a nuclear lamina component, lamin A/C, and LINC complex components SUN1, SUN2, and nesprin-2 in breast cancer. Cancer Med 4, 1547–1557. [PubMed: 26175118]
30. Gao J, Aksoy BA, Dogrusoz U, Dresdner G, Gross B, Sumer SO, Sun Y, Jacobsen A, Sinha R, Larsson E, et al. (2013). Integrative analysis of complex cancer genomics and clinical profiles using the cBioPortal. Sci Signal 6, pl1. [PubMed: 23550210]
31. Cerami E, Gao J, Dogrusoz U, Gross BE, Sumer SO, Aksoy BA, Jacobsen A, Byrne CJ, Heuer ML, Larsson E, et al. (2012). The cBio cancer genomics portal: an open platform for exploring multidimensional cancer genomics data. Cancer Discov 2, 401–404. [PubMed: 22588877]
32. Debnath J, and Brugge JS (2005). Modelling glandular epithelial cancers in three-dimensional cultures. Nat Rev Cancer 5, 675–688. [PubMed: 16148884]
33. Paszek MJ, Zahir N, Johnson KR, Lakins JN, Rozenberg GI, Gefen A, Reinhart-King CA, Margulies SS, Dembo M, Boettiger D, et al. (2005). Tensional homeostasis and the malignant phenotype. Cancer Cell 8, 241–254. [PubMed: 16169468]
34. Debnath J, Muthuswamy SK, and Brugge JS (2003). Morphogenesis and oncogenesis of MCF-10A mammary epithelial acini grown in three-dimensional basement membrane cultures. Methods 30, 256–268. [PubMed: 12798140]
35. Xiang B, and Muthuswamy SK (2006). Using three-dimensional acinar structures for molecular and cell biological assays. Methods Enzymol 406, 692–701. [PubMed: 16472698]
36. Zegers MM, O'Brien LE, Yu W, Datta A, and Mostov KE (2003). Epithelial polarity and tubulogenesis in vitro. Trends Cell Biol 13, 169–176. [PubMed: 12667754]
37. Bryant DM, Roignot J, Datta A, Overeem AW, Kim M, Yu W, Peng X, Eastburn DJ, Ewald AJ, Werb Z, et al. (2014). A molecular switch for the orientation of epithelial cell polarization. Dev Cell 31, 171–187. [PubMed: 25307480]
38. Bryant DM, and Mostov KE (2008). From cells to organs: building polarized tissue. Nat Rev Mol Cell Biol 9, 887–901. [PubMed: 18946477]
39. Neelam S, Chancellor TJ, Li Y, Nickerson JA, Roux KJ, Dickinson RB, and Lele TP (2015). Direct force probe reveals the mechanics of nuclear homeostasis in the mammalian cell. Proc Natl Acad Sci U S A 112, 5720–5725. [PubMed: 25901323]
40. Luxton GW, Gomes ER, Folker ES, Vintinner E, and Gundersen GG (2010). Linear arrays of nuclear envelope proteins harness retrograde actin flow for nuclear movement. Science 329, 956–959. [PubMed: 20724637]
41. Roux KJ, Crisp ML, Liu Q, Kim D, Kozlov S, Stewart CL, and Burke B (2009). Nesprin 4 is an outer nuclear membrane protein that can induce kinesin-mediated cell polarization. Proc Natl Acad Sci U S A 106, 2194–2199. [PubMed: 19164528]
42. Ostlund C, Folker ES, Choi JC, Gomes ER, Gundersen GG, and Worman HJ (2009). Dynamics and molecular interactions of linker of nucleoskeleton and cytoskeleton (LINC) complex proteins. J Cell Sci 122, 4099–4108. [PubMed: 19843581]
43. Sosa BA, Rothballer A, Kutay U, and Schwartz TU (2012). LINC complexes form by binding of three KASH peptides to domain interfaces of trimeric SUN proteins. Cell 149, 1035–1047. [PubMed: 22632968]
44. Mammoto T, Mammoto A, and Ingber DE (2013). Mechanobiology and developmental control. Annu Rev Cell Dev Biol 29, 27–61. [PubMed: 24099083]
45. Mammoto T, and Ingber DE (2010). Mechanical control of tissue and organ development. Development 137, 1407–1420. [PubMed: 20388652]
46. Moore KA, Polte T, Huang S, Shi B, Alsberg E, Sunday ME, and Ingber DE (2005). Control of basement membrane remodeling and epithelial branching morphogenesis in embryonic lung by Rho and cytoskeletal tension. Dev Dyn 232, 268–281. [PubMed: 15614768]
47. Lelièvre SA, Weaver VM, Nickerson JA, Larabell CA, Bhaumik A, Petersen OW, and Bissell MJ (1998). Tissue phenotype depends on reciprocal interactions between the extracellular matrix and the structural organization of the nucleus. Proc Natl Acad Sci U S A 95, 14711–14716. [PubMed: 9843954]
48. Weaver VM (2017). Cell and tissue mechanics: the new cell biology frontier. Mol Biol Cell 28, 1815–1818. [PubMed: 28684606]

49. Venugopalan G, Camarillo DB, Webster KD, Reber CD, Sethian JA, Weaver VM, Fletcher DA, El-Samad H, and Rycroft CH (2014). Multicellular architecture of malignant breast epithelia influences mechanics. PLoS One 9, e101955. [PubMed: 25111489]
50. Levental KR, Yu H, Kass L, Lakins JN, Egeblad M, Erler JT, Fong SF, Csiszar K, Giaccia A, Weninger W, et al. (2009). Matrix crosslinking forces tumor progression by enhancing integrin signaling. Cell 139, 891–906. [PubMed: 19931152]
51. Curran S, Strandkvist C, Bathmann J, de Gennes M, Kabla A, Salbreux G, and Baum B (2017). Myosin II Controls Junction Fluctuations to Guide Epithelial Tissue Ordering. Dev Cell 43, 480–492.e486. [PubMed: 29107560]
52. Kassianidou E, Hughes JH, and Kumar S (2017). Activation of ROCK and MLCK tunes regional stress fiber formation and mechanics via preferential myosin light chain phosphorylation. Mol Biol Cell 28, 3832–3843. [PubMed: 29046396]
53. Joo EE, and Yamada KM (2014). MYPT1 regulates contractility and microtubule acetylation to modulate integrin adhesions and matrix assembly. Nat Commun 5, 3510. [PubMed: 24667306]
54. Wu C, Asokan SB, Berginski ME, Haynes EM, Sharpless NE, Griffith JD, Gomez SM, and Bear JE (2012). Arp2/3 is critical for lamellipodia and response to extracellular matrix cues but is dispensable for chemotaxis. Cell 148, 973–987. [PubMed: 22385962]
55. Goeckeler ZM, Bridgman PC, and Wysolmerski RB (2008). Nonmuscle myosin II is responsible for maintaining endothelial cell basal tone and stress fiber integrity. Am J Physiol Cell Physiol 295, C994–1006. [PubMed: 18701651]
56. Pearson GW, and Hunter T (2007). Real-time imaging reveals that noninvasive mammary epithelial acini can contain motile cells. J Cell Biol 179, 1555–1567. [PubMed: 18166657]
57. Kasza KE, Rowat AC, Liu J, Angelini TE, Brangwynne CP, Koenderink GH, and Weitz DA (2007). The cell as a material. Curr Opin Cell Biol 19, 101–107. [PubMed: 17174543]
58. Peterson LJ, Rajfur Z, Maddox AS, Freel CD, Chen Y, Edlund M, Otey C, and Burridge K (2004). Simultaneous stretching and contraction of stress fibers in vivo. Mol Biol Cell 15, 3497–3508. [PubMed: 15133124]
59. Watanabe T, Hosoya H, and Yonemura S (2007). Regulation of myosin II dynamics by phosphorylation and dephosphorylation of its light chain in epithelial cells. Mol Biol Cell 18, 605–616. [PubMed: 17151359]
60. Sumida GM, Tomita TM, Shih W, and Yamada S (2011). Myosin II activity dependent and independent vinculin recruitment to the sites of E-cadherin-mediated cell-cell adhesion. BMC Cell Biol 12, 48. [PubMed: 22054176]
61. Tiwari N, Gheldof A, Tatari M, and Christofori G (2012). EMT as the ultimate survival mechanism of cancer cells. Semin Cancer Biol 22, 194–207. [PubMed: 22406545]
62. Chancellor TJ, Lee J, Thodeti CK, and Lele T (2010). Actomyosin tension exerted on the nucleus through nesprin-1 connections influences endothelial cell adhesion, migration, and cyclic strain-induced reorientation. Biophys J 99, 115–123. [PubMed: 20655839]
63. Heo SJ, Driscoll TP, Thorpe SD, Nerurkar NL, Baker BM, Yang MT, Chen CS, Lee DA, and Mauck RL (2016). Differentiation alters stem cell nuclear architecture, mechanics, and mechano-sensitivity. Elife 5.
64. Alam SG, Zhang Q, Prasad N, Li Y, Chamala S, Kuchibhotla R, Kc B, Aggarwal V, Shrestha S, Jones AL, et al. (2016). The mammalian LINC complex regulates genome transcriptional responses to substrate rigidity. Sci Rep 6, 38063. [PubMed: 27905489]
65. Zhang Q, Kota KP, Alam SG, Nickerson JA, Dickinson RB, and Lele TP (2016). Coordinated Dynamics of RNA Splicing Speckles in the Nucleus. J Cell Physiol 231, 1269–1275. [PubMed: 26496460]
66. Armiger TJ, Lampi MC, Reinhart-King CA, and Dahl KN (2018). Determining mechanical features of modulated epithelial monolayers using subnuclear particle tracking. J Cell Sci 131.
67. Alam SG, Lovett D, Kim DI, Roux KJ, Dickinson RB, and Lele TP (2015). The nucleus is an intracellular propagator of tensile forces in NIH 3T3 fibroblasts. J Cell Sci 128, 1901–1911. [PubMed: 25908852]
68. Cain NE, Jahed Z, Schoenhofen A, Valdez VA, Elkin B, Hao H, Harris NJ, Herrera LA, Woolums BM, Mofrad MRK, et al. (2018). Conserved SUN-KASH Interfaces Mediate LINC Complex-

Dependent Nuclear Movement and Positioning. Curr Biol 28, 3086–3097.e3084. [PubMed: 30245107]

69. Gimpel P, Lee YL, Sobota RM, Calvi A, Koullourou V, Patel R, Mamchaoui K, Nédélec F, Shackleton S, Schmoranzer J, et al. (2017). Nesprin-1α-Dependent Microtubule Nucleation from the Nuclear Envelope via Akap450 Is Necessary for Nuclear Positioning in Muscle Cells. Curr Biol 27, 2999–3009.e2999. [PubMed: 28966089]
70. Lee YL, and Burke B (2018). LINC complexes and nuclear positioning. Semin Cell Dev Biol 82, 67–76. [PubMed: 29191370]
71. Lele TP, Dickinson RB, and Gundersen GG (2018). Mechanical principles of nuclear shaping and positioning. J Cell Biol.
72. Hale CM, Shrestha AL, Khatau SB, Stewart-Hutchinson PJ, Hernandez L, Stewart CL, Hodzic D, and Wirtz D (2008). Dysfunctional connections between the nucleus and the actin and microtubule networks in laminopathic models. Biophys J 95, 5462–5475. [PubMed: 18790843]
73. Khatau SB, Hale CM, Stewart-Hutchinson PJ, Patel MS, Stewart CL, Searson PC, Hodzic D, and Wirtz D (2009). A perinuclear actin cap regulates nuclear shape. Proc Natl Acad Sci U S A 106, 19017–19022. [PubMed: 19850871]
74. Uhler C, and Shivashankar GV (2018). Nuclear Mechanopathology and Cancer Diagnosis. Trends Cancer 4, 320–331. [PubMed: 29606315]
75. Thakar K, May CK, Rogers A, and Carroll CW (2017). Opposing roles for distinct LINC complexes in regulation of the small GTPase RhoA. Mol Biol Cell 28, 182–191. [PubMed: 28035049]
76. May CK, and Carroll CW (2018). Differential incorporation of SUN-domain proteins into LINC complexes is coupled to gene expression. PLoS One 13, e0197621. [PubMed: 29813079]
77. Samuel MS, Lopez JI, McGhee EJ, Croft DR, Strachan D, Timpson P, Munro J, Schröder E, Zhou J, Brunton VG, et al. (2011). Actomyosin-mediated cellular tension drives increased tissue stiffness and β-catenin activation to induce epidermal hyperplasia and tumor growth. Cancer Cell 19, 776–791. [PubMed: 21665151]
78. Lombardi ML, Jaalouk DE, Shanahan CM, Burke B, Roux KJ, and Lammerding J (2011). The interaction between nesprins and sun proteins at the nuclear envelope is critical for force transmission between the nucleus and cytoskeleton. J Biol Chem 286, 26743–26753. [PubMed: 21652697]
79. Meerbrey KL, Hu G, Kessler JD, Roarty K, Li MZ, Fang JE, Herschkowitz JI, Burrows AE, Ciccia A, Sun T, et al. (2011). The pINDUCER lentiviral toolkit for inducible RNA interference in vitro and in vivo. Proc Natl Acad Sci U S A 108, 3665–3670. [PubMed: 21307310]
80. Tiscornia G, Singer O, and Verma IM (2006). Production and purification of lentiviral vectors. Nat Protoc 1, 241–245. [PubMed: 17406239]
81. Gayrard C, Bernaudin C, Déjardin T, Seiler C, and Borghi N (2018). Src- and confinement-dependent FAK activation causes E-cadherin relaxation and β-catenin activity. J Cell Biol 217, 1063–1077. [PubMed: 29311227]
82. Schulze KD, Zehnder SM, Urueña JM, Bhattacharjee T, Sawyer WG, and Angelini TE (2017). Elastic modulus and hydraulic permeability of MDCK monolayers. J Biomech 53, 210–213. [PubMed: 28173919]
83. Lee GY, Kenny PA, Lee EH, and Bissell MJ (2007). Three-dimensional culture models of normal and malignant breast epithelial cells. Nat Methods 4, 359–365. [PubMed: 17396127]
84. Schneider CA, Rasband WS, and Eliceiri KW (2012). NIH Image to ImageJ: 25 years of image analysis. Nat Methods 9, 671–675. [PubMed: 22930834]
85. Muranen T, Selfors LM, Worster DT, Iwanicki MP, Song L, Morales FC, Gao S, Mills GB, and Brugge JS (2012). Inhibition of PI3K/mTOR leads to adaptive resistance in matrix-attached cancer cells. Cancer Cell 21, 227–239. [PubMed: 22340595]
86. Team RC (2018). R: A language and environment for statistical computing (Vienna, Austria: R Foundation for Statistical Computing).

Highlights:

- The LINC complex is required for normal development of epithelial acini with lumens
- LINC complex disruption increases myosin regulatory light chain phosphorylation
- Increased myosin activity causes collapse of the dynamically fluctuating acinus
- The LINC complex mechanically stabilizes the epithelial acinus

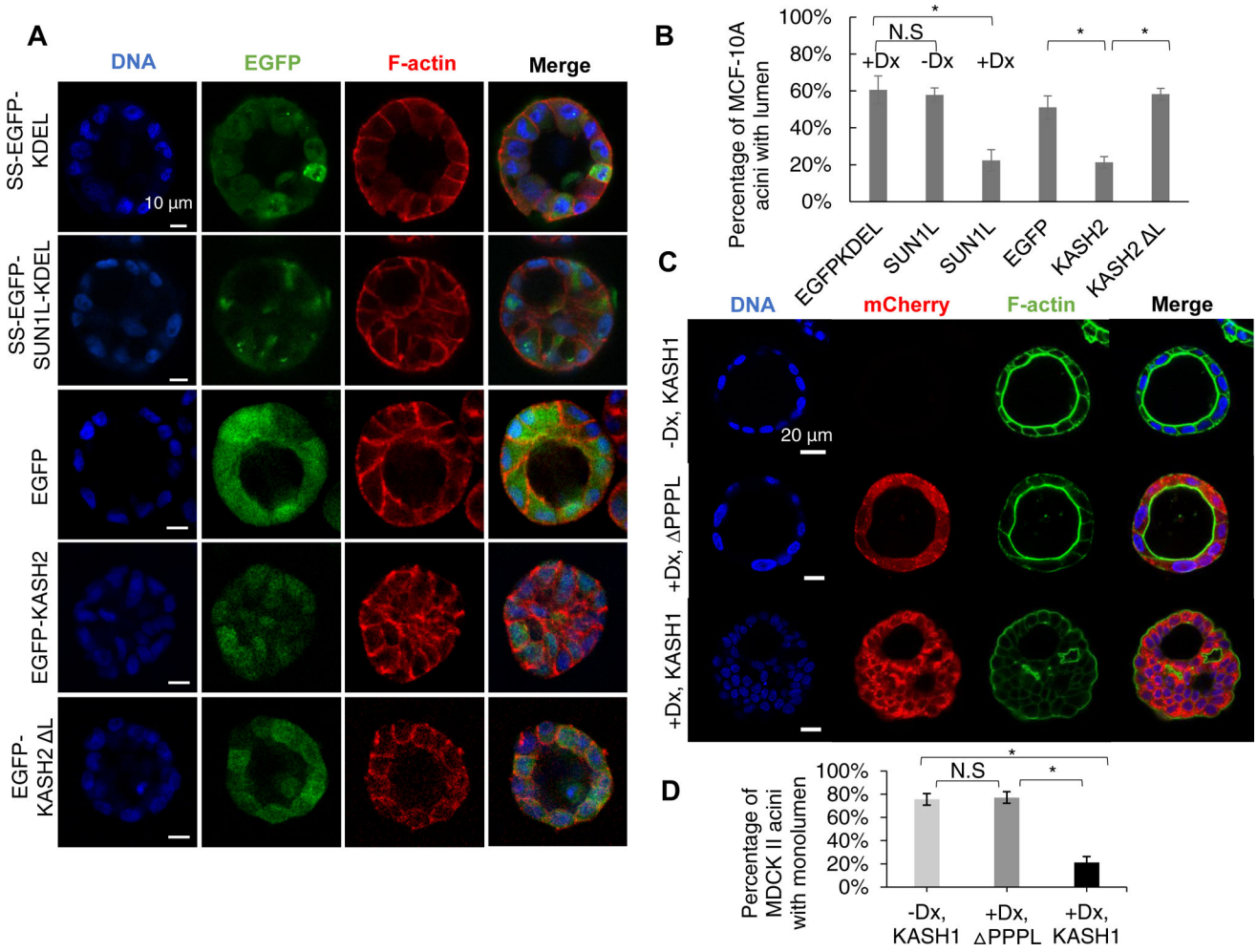

Figure 1. Disruption of the LINC complex results in lumen occlusion during acinar development by MCF-10A and MDCK II cells.

LINC complex disruption was induced by doxycycline before seeding on the Matrigel™. (**A**) Fluorescent images of representative acini formed by MCF-10A cells expressing the proteins indicated in the left column. Scale bar, 10 mm. (**B**) Occurrence of MCF-10A acini with a lumen under different conditions presented in (**A**). EGFPKDEL: SS-EGFP-KDEL, SUN1L: SS-EGFP-SUN1L-KDEL (-Dx, without doxycycline, +Dx, with doxycycline), KASH2: EGFP-KASH2, KASH2 ΔL: EGFP-KASH2. If one or more cells were observed inside the three-dimensional lumen, as visualized using *z*-stack confocal microscopy, the acinus was scored as lacking a lumen; n ≥ 93 acini from at least three experiments for each condition. Error bars represent ± SEM (* $p < 0.05$, Student's *t*-test with Bonferroni corrections). (**C**) Fluorescent images of representative acini formed over a period of 7 days by uninduced MDCK II cells (-Dx, KASH1), by MDCK II cells inducibly expressing mCherry-KASH1ΔPPPL induced with doxycycline on day −1 (+Dx, DPPPL) or by MDCK II cells inducibly expressing mCherry-KASH1 induced with doxycycline on day −1 (+Dx, KASH1). DNA and F-actin were imaged through Hoechst and phalloidin staining respectively. Scale bar, 20 μm. (**D**) Occurrence of MDCK II acini with a single lumen under different conditions in (**E**). n≥120 acini from 3 independent experiments for each condition.

Error bars represent ± SEM (*p<0.001, One-Way ANOVA with post-hoc Tukey (HSD) test). Also see Figure S1 and S2 for validation of LINC complex disruption.

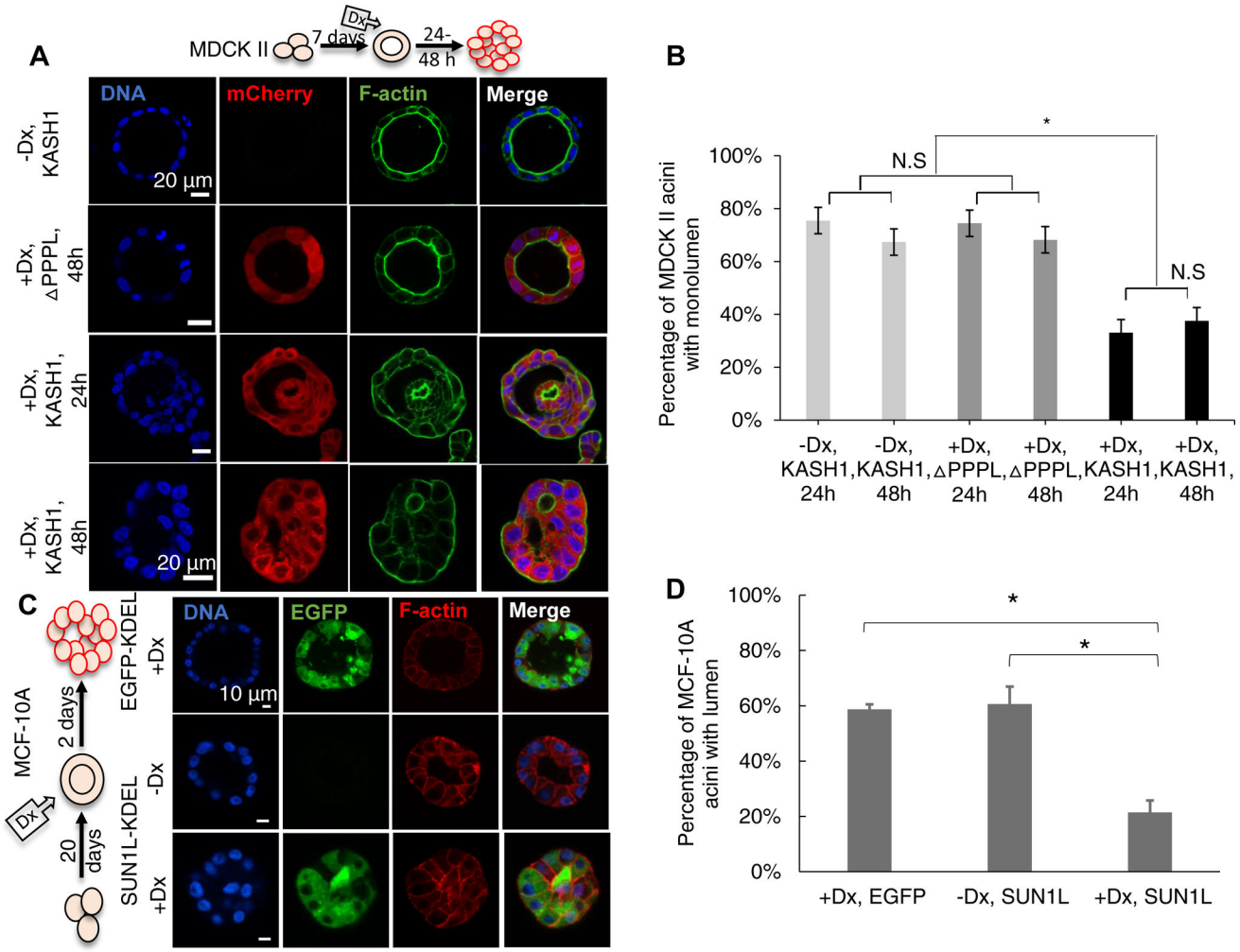

Figure 2. Disruption of the LINC complex induces lumen blockage in pre-formed MCF-10A and MDCK II acini.

Non-induced cells were allowed to form acini; then doxycycline (Dx) was added to induce expression of ΔPPPL: mCherry-KASHΔPPPL and KASH1: mCherry-KASH1 (**A**) or EGFP-KDEL: SS-EGFP-KDEL and SUN1L-KDEL: SS-EGFP-SUN1L-KDEL (**C**). The cartoon in (**A**) and (**C**) indicates the period of three-dimensional culture (7 d for MDCK II cells, 20 d for MCF-10A cells), and the duration of induction by doxycycline before acinar fixation and microscopy (1–2 d for MDCK II acini, 2 d for MCF-10A acini). (**B**) Plot shows occurrence of MDCK II acini with single lumen corresponding to the data in (**A**). n ≥100 acini from 3 independent experiments were scored for each group. Error bars represent ± SEM (*$p <$ 0.001, and N.S. (not significant) by one-way ANOVA followed by Tukey (HSD) test for multiple comparisons). (**D**) Plot shows the occurrence of MCF-10A acini with lumens under different conditions corresponding to the data in (**C**). At least 80 acini from 3 independent experiments were scored for each group. Error bars represent ± SEM (*p<0.05 by student's t-test with Bonferroni corrections for statistical comparisons).

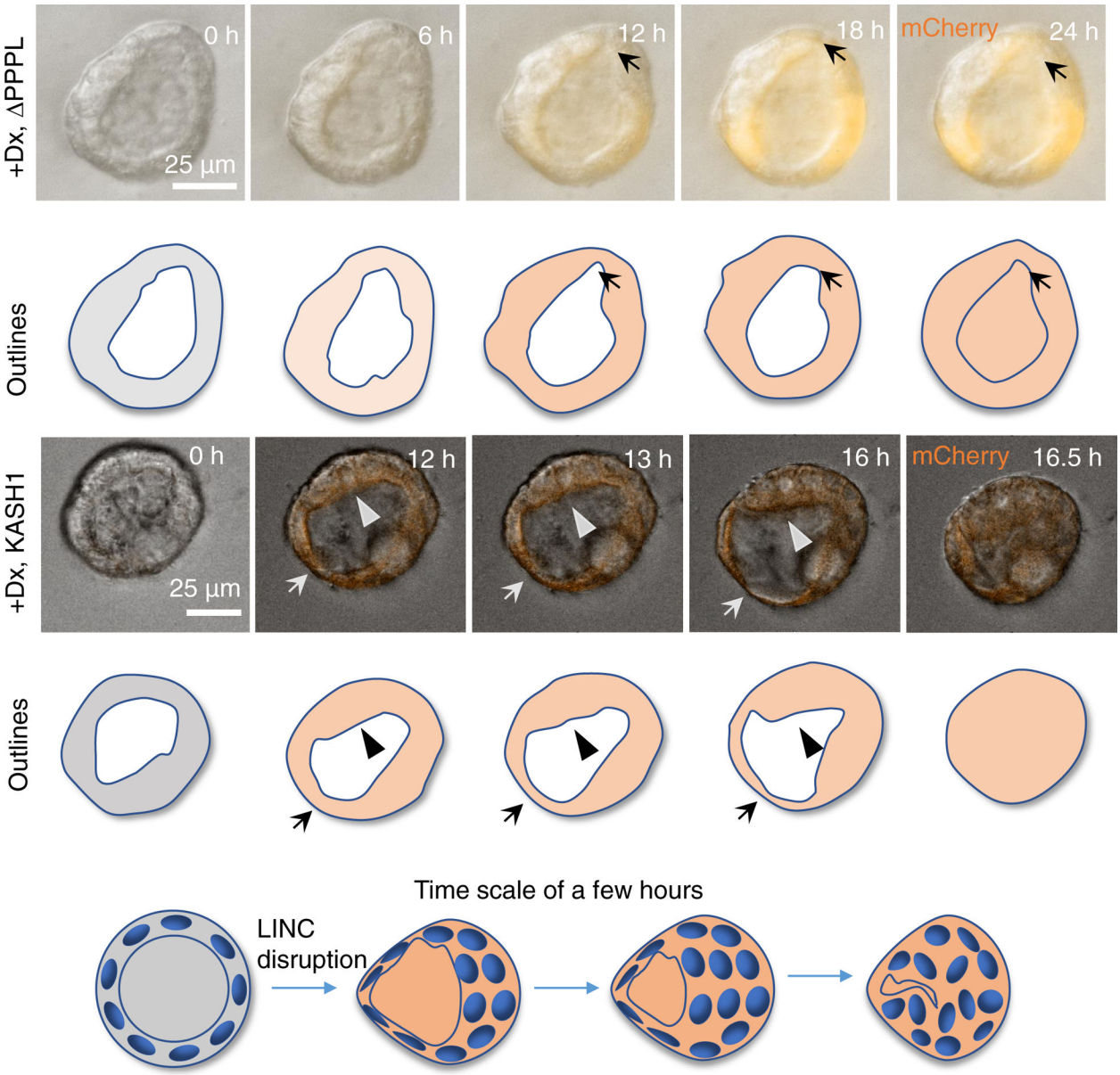

Figure 3. LINC disruption destabilizes the acinus.

Time-lapse differential interference contrast (DIC) microscopy images overlaid with fluorescent images of mCherry-KASH1ΔPPPL (+Dx, ΔPPPL) or mCherry-KASH1 (+Dx, KASH1) showing shape fluctuations of the MDCK II cell acinar boundaries and corresponding outlines (the expression of either protein was induced by doxycycline, Dx, added at time = 0 h) (see also Video S1). In the top panel, local thinning is observed (arrow, starting at 12 h) in the control acinus, which recovers by 18 h. Such thinning/thickening followed by recovery was seen in 23 acini that did not collapse out of 23 assayed mCherry-KASH1ΔPPPL acini from 6 different experiments. Conversely, in the mCherry-KASH1 acinus, there is thinning (arrow) and thickening (arrowheads), at the opposite poles. The thick boundary continues to thicken, moves inward, and eventually meets the thin boundary, resulting in acinar collapse (after 16 h) (see also Videos S2, S3 and S4). The thick boundary

covers the distance of the acinar radius in approximately 3 h to collapse the acinus. Such collapse was observed in 35 acini out of 50 assayed acini in 5 different experiments. The model shows how the local thinning and thickening of cells result in lumenal collapse in pre-developed acini formed by LINC disrupted MDCK II cells. Cell boundaries are not shown in the cartoon. See also Figure S3 for the effect of LINC complex disruption on the geometric properties of MCF-10A and MDCKII acini.

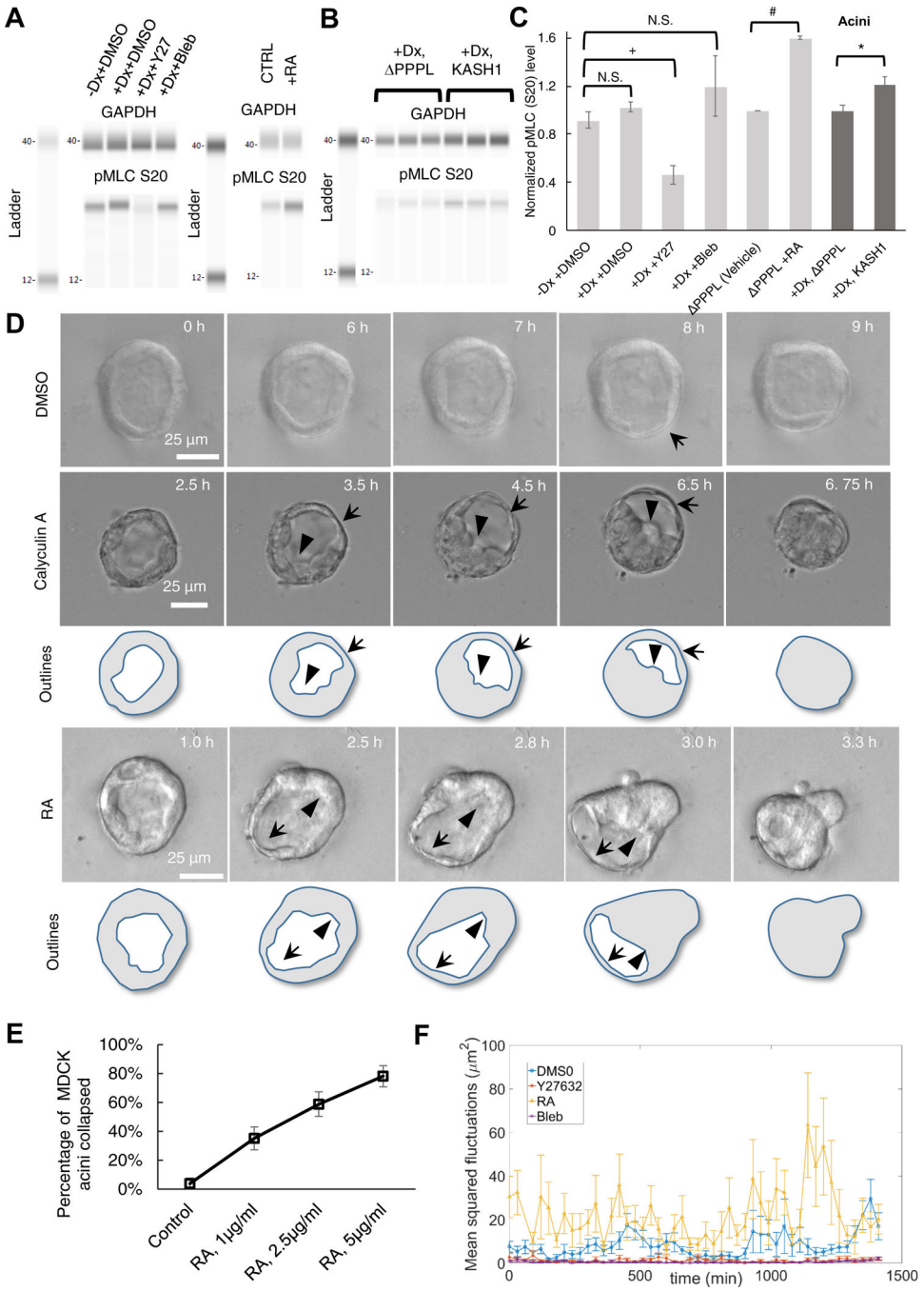

Figure 4. Levels of phosphorylated myosin II regulatory light chain (pMLC) increase upon LINC complex disruption in acini, and increased actomyosin contractility causes lumenal collapse.

(**A**) Western blot of pMLC levels detected using anti-myosin light chain (phospho S20) antibody in lysates from MDCK II cells cultured in two-dimensional tissue culture dishes. +Dx indicates doxycycline treatment for 1 day to induce the expression of mCherry-KASH1. The effect of 40 µM Y27632 (Y27), 50 µM blebbistatin (Bleb) treatment on pMLC levels are shown; DMSO was included as vehicle control. Also shown is the effect of 1 µg/ml Rho activator II treatment. GAPDH was used as loading control; N ≥ 4 per condition

(except Rho activator II, where N = 2). (**B**) Western blot analysis of pMLC levels detected using anti-Myosin light chain (phospho S20) antibody from MDCK II acini formed through culture in three-dimensional Matrigel™. Doxycycline (Dx) was added to induce expression of mCherry-KASH1ΔPPPL and mCherry-KASH1 for 1 day before seeding cells in Matrigel™, and cells were harvested from acini after 7 days. GAPDH was used as loading control and N = 6 biological replicates were assayed. See also Figure S4 for immunofluorescence data with the anti-Myosin light chain (phospho S20) antibody. (**C**) Plot shows the normalized pMLC levels corresponding to the data in (a) and (b). Error bars indicate ± SEM (*p<0.05 by student's t-test for statistical comparisons with Bonferroni corrections for multiple comparisons). (**D**) Time-lapse DIC and fluorescent images of acini formed over 7 days in three-dimensional culture by uninduced MDCK II cells, followed by treatment with DMSO (vehicle control), 5 nM calyculin A (see Videos S5 and S6) or 2.5 μg/ml Rho activator II (see also Video S7) at time = 0 h. Images are representative of 40 acini that did not collapse out of 43 assayed in 6 different experiments under DMSO treatment, 31 acini that collapsed out of 31 assayed under Calyculin A treatment in 3 different experiments, and 20 acini that collapsed out of 34 assayed under Rho activator II treatment in 3 different experiments. Local thinning is indicated by arrows and local thickening by arrowheads. (**E**) Plot shows the percentage of acini that collapsed as a function of the dose of Rho activator II (RA). At least 26 acini from 3 independent experiments were assayed for each dose. (**F**) Plot shows the mean squared fluctuations in acinar thickness (quantified at two locations in each acinus) in uninduced mCherry-KASH1 cells treated with 40μM Y27632, 1 μg/ml Rho activator II (see Video S8) or 50 μM Blebbistatin (see Video S9). DMSO served as vehicle control. Data in the plot represents results from live imaging of at least 6 acini from 3 independent experiments, corresponding to at least 12 time series for each condition.

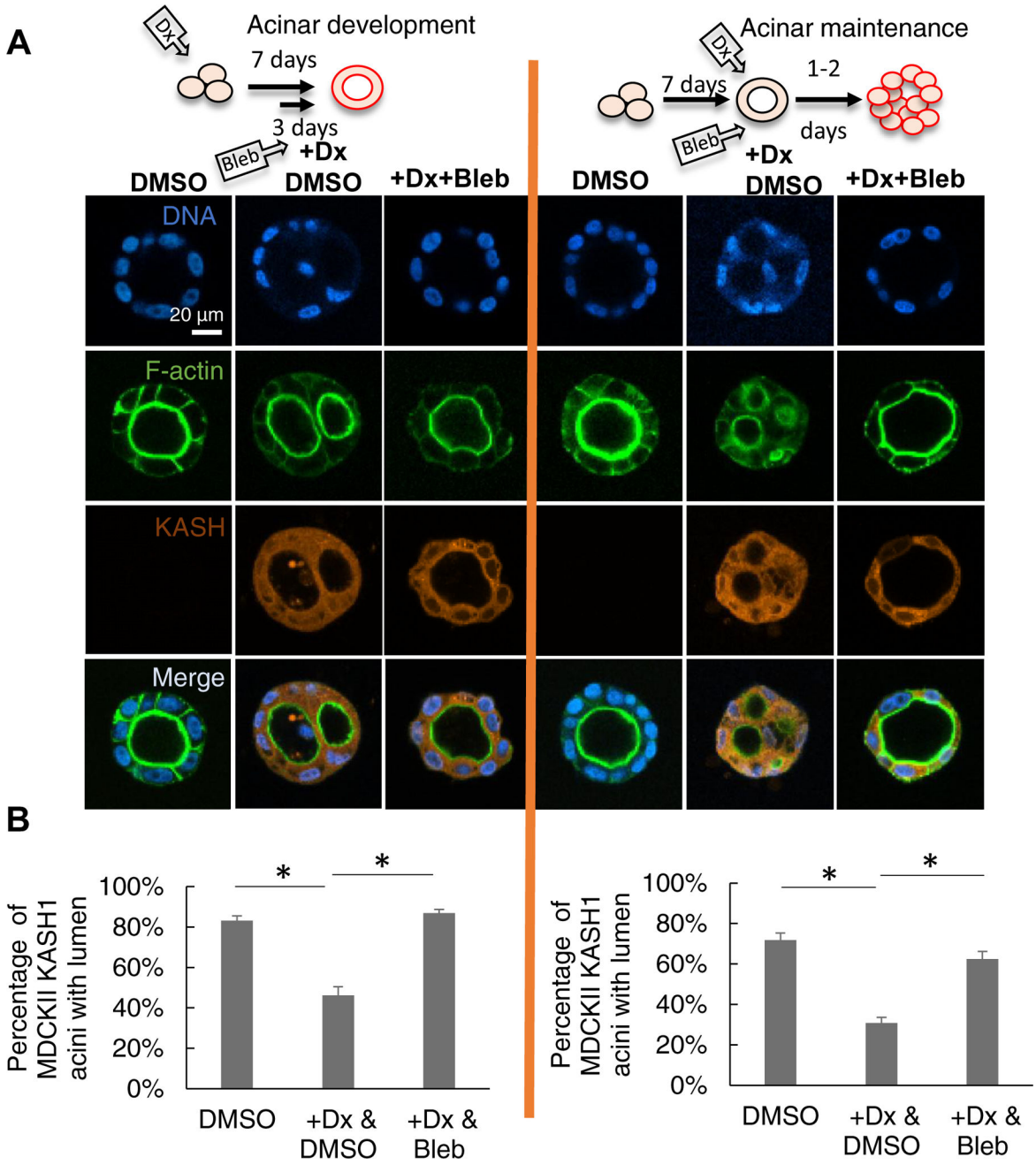

Figure 5. Inhibition of NMMII motor activity rescues lumen formation and prevents lumen blockage.

(**A**) Fluorescent images of representative MDCK II acini formed under the indicated conditions. +Dx&DMSO: doxycycline treatment inducing the expression of mCherry-KASH1; DMSO was included as vehicle control; +Dx&Bleb: doxycycline treatment to induce mCherry-KASH1 expression followed by blebbistatin treatment to inhibit NMMII. In the left panel (acinar development), doxycycline was added at 0 d, acini allowed to develop for 7 d in Matrigel™ with blebbistatin added on day 4 (+Dx+Bleb) or without blebbistatin (+Dx). DMSO is the untreated control with DMSO. In the right panel (acinar maintenance), uninduced MDCK II cells were allowed to form acini for 7 d (-Dx, DMSO added at day 7),

and were then treated with doxycycline for 2 d (+Dx, DMSO added at day 7 with doxycycline), or with doxycycline and blebbistatin (+Dx+Bleb). DMSO: addition of DMSO after the 7^{th} day for two days. (**B**) Quantitative analysis of data from (**A**). At least 190 acini from at least three experiments were analyzed for each condition. Error bars represent ± SEM (* $p < 0.05$, Student's *t*-test with Bonferroni corrections for multiple comparisons). The cartoon on the top of each panel indicates the period of three-dimensional culture and period of blebbistatin addition. Dx: doxycycline.

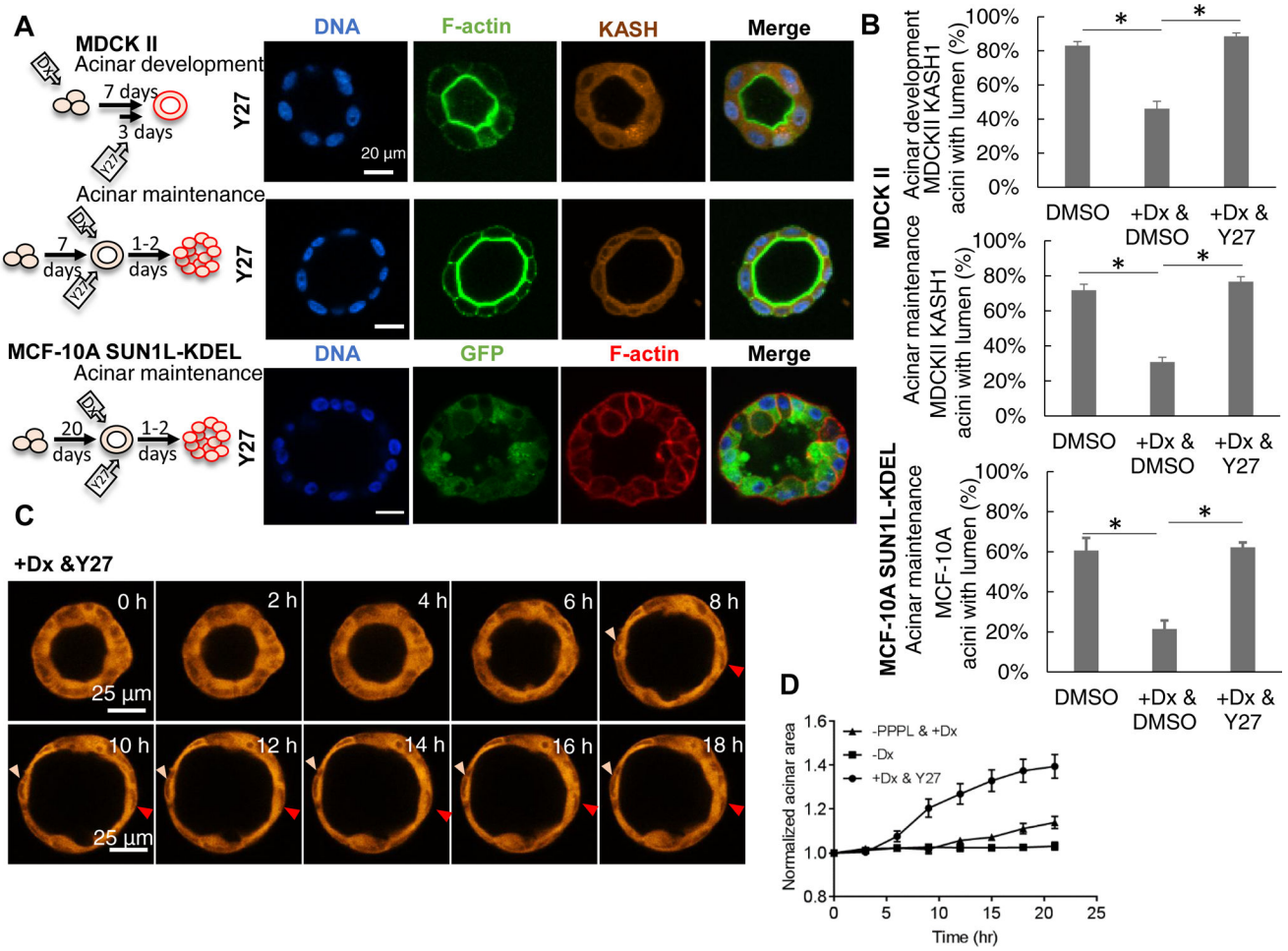

Figure 6. ROCK inhibition rescues the lumen phenotype and causes acinar expansion.

(**A**) Fluorescent images of representative acini formed by MDCK II cells induced for 7 d with doxycycline to induce mCherry-KASH1, and with ROCK inhibitor Y27632 (Y27) added on day 4 of culture (top panel, acinar development); images of acini formed during 7-d culture, followed by 2-d treatment with doxycycline to induce mCherry-KASH1 expression and Y27632 to inhibit ROCK (middle panel, acinar maintenance); and images of acini formed by uninduced MCF-10A cells followed by 2-d treatment with doxycycline to induce EGFP-SUN1L-KDEL expression and Y27632 to inhibit ROCK (bottom panel). The cartoon next to each panel indicates the period of three-dimensional culture and Y27632 treatment. Dx: doxycycline. (**B**) Quantification of data corresponding to (**A**) and untreated controls. DMSO served as vehicle control. At least 80 acini from at least three experiments were analyzed for the corresponding images in (**A**). Error bars represent ± SEM (* $p<0.05$, Student's t-test with Bonferroni corrections for multiple comparisons). (**C**) Time-lapse fluorescent images of an acinus formed by MDCK II cells expressing mCherry-KASH1, which was treated with 40 µM Y27632 at 0 h (see Video S10). The size of the acinus increases and the thickness of the acinus decreases over a period of several hours after Y27632 treatment. Two nuclei (arrowheads) do not move significantly in the images for several hours after reaching the expanded state. (**D**) Plot shows time-dependent, pooled,

averaged area and thickness of uninduced MDCK II acini (squares) normalized to the initial area and thickness respectively. Acini, pre-formed for 6 d, were induced with doxycycline for 24 hours to express mCherry-KASHΔPPPL (circles), or induced with doxycycline (Dx) for 24 h to express mCherry-KASH1 followed by 40 μM Y27632. The uninduced control is also shown. At least 5 acini from 3 experiments were analyzed, error bars are ± SEM.

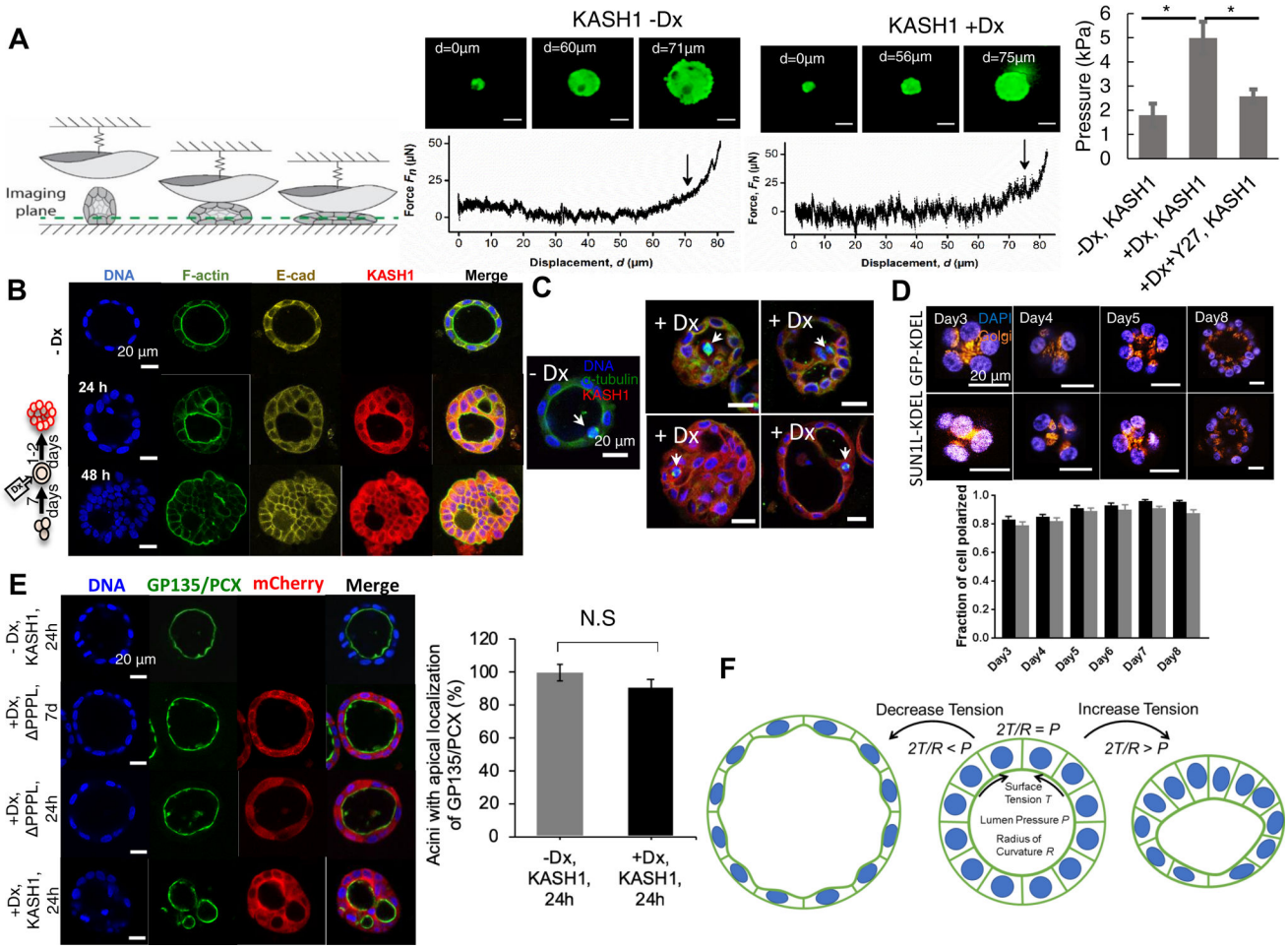

Figure 7. LINC disruption causes abnormal acinar mechanics and orientation of cell division but not acinar polarity.

(**A**) Schematic illustration of acinar indentation experiments, demonstrating how isolated acini indented using a glass hemisphere probe undergo large deformations. The normal force applied by the probe was measured while confocal fluorescent images were acquired simultaneously of the MDCK II acini (acini were treated with calcein (green)). Representative fluorescent images and corresponding indentation curves showing the initial deformation of representative MDCK II acini, followed by blebbing and/or rupture of the acinar surface. The applied pressure at which blebbing/rupture occurred was determined from the simultaneous measurement of the contact area and force. Arrows designate the normal force at which failure occurred. Scale bars, 50 mm. –Dx, KASH1: uninduced MDCK II acini; +Dx, KASH1: MDCK II acini treated with doxycycline at day 0 to induce expression of mCherry-KASH1 and allowed to develop for 7 days; +Dx+Y27, MDCK II acini treated with doxycycline at day 0 to induce expression of mCherry-KASH1, 40 μM Y27632 was added at day 4 of the 7 d culture. Bar plot shows the effect of doxycycline-induced mCherry-KASH1 expression on the pressure at which the acini bleb/rupture, in the presence or absence of Y27632 (added at day 4 of the 7d culture). Error bars represent ± SEM (*p <0.05, Student's t-test with Bonferroni correction). At least 8 acini cultured from at least two independent experiments were analyzed per condition. **(B)** Already developed

MDCK II acini were treated with doxycycline to express mCherry-KASH1 on day 7 of culture, and fixed 24 h and 48 h post-doxycycline treatment (+Dx). Images show overlays of immunostained F-actin (green), E-cadherin (yellow), mCherry-KASH1 (red) and DNA (blue; stained with Hoechst). Scale bar, 20 mm. **(C)** Already developed MDCK II acini were treated with doxycycline to express mCherry-KASH1 on day 7 of culture, and fixed 24 h post-doxycycline treatment (+Dx). Images show overlays of immunostained alpha-tubulin (green), mCherry-KASH1 (red) and DNA (blue; stained with Hoechst). Scale bar, 20 mm. (**D**) Fluorescent images show representative acini formed by EGFP-KDEL cells (top) and SUN1LKDEL cells (bottom) stained with DAPI and for GM130 (labeling Golgi) at different days after induction; cells were induced with doxycycline at day −2. Scale bar, 20 μm. Bar plot shows the fraction of acini that are polarized (acini with the Golgi between the developing lumen and the nuclei were scored as polarized) at different days. Error bars represent ± SEM; at least 195 nuclei were scored from 3 different experiments at each condition and time point. No statistically significant differences were observed between EGFP-KDEL and SUN1L-KDEL acini based on Student t-test. (**E**) Fluorescent images show representative acini in uninduced mCherry-KASH1 (-Dx), induced mCherry-KASH1ΔPPPL cultured in Matrigel for 7 days (+Dx, ΔPPPL, 7 d), preformed mCherry-KASH1ΔPPPL acini induced with doxycycline for 24 hr (+Dx, ΔPPPL, 24 hr) and preformed mCherry-KASH1 acini induced with doxycycline for 24 hr stained with Hoechst (blue) and for gp135 (green) (+Dx, KASH1, 24h). Scale bar, 20 μm. Plot shows the percentage of MDCKII acini with apical localization of gp135. At least 120 acini from 3 experiments were scored for each condition. Error bars represent ± SEM. No statistical significance was detected based on Student t-test. (**F**) Mechanical model for acinar maintenance. Decrease in NMMII generated tension results in expansion of the acinus (left) and increase in NMMII tension due to LINC disruption results in compression of the acinus and lumen collapse.